Development of an analytical solution of modified Biot's equations for the optimization of lightweight acoustic protection

Jamil Kanfoud[a)] and Mohamed Ali Hamdi
Laboratoire Roberval, Université de Technologie de Compiegne, Rue Personne de Roberval,
Centre de Recherche CRD338, B.P. 20529, Compiegne Cedex 60205, France

François-Xavier Becot and Luc Jaouen
MATELYS - Acoustique and Vibrations, 20/24 rue Robert Desnos, F-69120 Vaulx-en-Velin, France

During lift-off, space launchers are submitted to high-level of acoustic loads, which may damage sensitive equipments. A special acoustic absorber has been previously integrated inside the fairing of space launchers to protect the payload. A new research project has been launched to develop a low cost fairing acoustic protection system using optimized layers of porous materials covered by a thin layer of fabric. An analytical model is used for the analysis of acoustic wave propagation within the multilayer porous media. Results have been validated by impedance tube measurements. A parametric study has been conducted to determine optimal mechanical and acoustical properties of the acoustic protection under dimensional thickness constraints. The effect of the mounting conditions has been studied. Results reveal the importance of the lateral constraints on the absorption coefficient particularly in the low frequency range. A transmission study has been carried out, where the fairing structure has been simulated by a limp mass layer. The transmission loss and noise reduction factors have been computed using Biot's theory and the local acoustic impedance approximation to represent the porous layer effect. Comparisons between the two models show the frequency domains for which the local impedance model is valid.
© 2009 Acoustical Society of America. [DOI: 10.1121/1.2973197]

I. INTRODUCTION

The purpose of this paper is to develop an analytical model permitting the solution of Biot's equations governing wave propagation for planar elastic porous layers. The study aims to design an optimized acoustic protection having a high acoustic absorption coefficient (AC) in the very low frequency band (the 63 Hz third octave band). As described in Refs. 1–5, original Biot's equations have been written in terms of solid and fluid displacements. In Ref. 6, Bonnet derived basic singular solutions of Biot's equations. By eliminating the fluid displacement, he established a system of four differential equations coupling the skeleton displacement and the acoustic pressure in the interstitial fluid. For finite element implementation purposes, a mixed displacement pressure integral formulation has been derived by Atalla *et al.*[7] Boundary conditions associated with the weak mixed displacement pressure formulation are discussed in Ref. 8. Previous papers assume that Biot's parameters are spatially constant. A modified system of four Biot's equations, valid for nonspatially constant Biot's parameters, was established by Hamdi *et al.* in Ref. 9. As described in Refs. 9 and 10, the weak formulation associated with modified Biot's equations has the great advantage of leading to natural boundary conditions at interfaces between adjacent layers.

To clarify the approach, the first section of the paper recalls the system of modified Biot's equations established in Ref. 9 in terms of the skeleton displacement vector and of the pressure inside the interstitial acoustic medium saturating the pores.

The second section derives analytical solutions of the modified Biot's equations propagating in planar and laterally infinite porous layers of finite thickness. Boundary conditions associated with the system of four differential equations are specified at interfaces between adjacent porous layers and at the interfaces between the porous layers and the fluid gaps. The case of a heavy septum covering porous layers is also studied.

The global analytical solution is derived for the case of an incident acoustic plane wave.

The third section is dedicated to the calculation and optimization of the acoustic AC with respect to Biot's parameters and the thickness of porous layers. A new absorber composed of a foam layer covered by a thin fabric has been optimized using the proposed analytical model. The results of the analytical study are validated using impedance tube measurements showing the effects of mounting conditions.

The fourth section of the paper is dedicated to calculations of the transmission loss (TL) factor of an impervious limp mass layer covered by a porous layer and of the noise reduction (NR) factor corresponding to two limp mass layers covered by the optimized porous layers and coupled by an air gap. Interesting new results, showing a comparison of TL

---
a)Electronic mail: jkanfoud@utc.fr

and NR curves obtained with the classical local acoustic impedance (LAI) and Biot's models, are presented at the end of this section. Finally, the last section concludes the paper and gives a perspective of the present research work.

II. THE MODIFIED BIOT EQUATIONS

Standard Biot equations [Eqs. (1a), (1b), (2a), and (2b)] written in terms of the skeleton displacement vector (U^s) and the fluid displacement vector (U^f) are the following:

$$(\hat{\rho}_s \ddot{U}^s + \hat{\rho}_{sf} \ddot{U}^f) = \nabla \cdot \sigma^s - b(\dot{U}^s - \dot{U}^f), \quad (1a)$$

$$(\hat{\rho}_{sf} \ddot{U}^s + \hat{\rho}_f \ddot{U}^f) = \nabla \cdot \sigma^f - b(\dot{U}^f - \dot{U}^s), \quad (1b)$$

where $\dot{U}$ and $\ddot{U}$ correspond to the velocity and acceleration vectors of the solid (s) and fluid (f) phases and σ^s and σ^f are, respectively, the solid and fluid stress tensors given in Ref. 2 by

$$\sigma^s_{ij} = \left[\left(P - \frac{2\mu}{3} \right) \nabla \cdot U^s + Q \nabla \cdot U^s \right] \delta_{ij}$$
$$+ \mu \left[\frac{\partial U^s_i}{\partial x_j} + \frac{\partial U^s_j}{\partial x_i} \right], \quad (2a)$$

$$\sigma^f_{ij} = -\phi p \delta_{ij} = [Q \nabla \cdot U^s + R \nabla \cdot U^s] \delta_{ij}, \quad (2b)$$

where μ is the shear modulus of the skeleton elastic material, and P, Q, and R are the bulk moduli of the porous media. According to Ref. 2, they are related to the bulk modulus K_s of the skeleton elastic material, to the bulk modulus K_f of the interstitial fluid, to the bulk modulus K_b of the porous frame at constant pressure in the air, and to the porosity ϕ by the following expressions:

$$P = \frac{(1-\phi)(1-\phi-K_b/K_s)K_s + \phi K_s K_b/K_f}{1-\phi-K_b/K_s + \phi K_s/K_f}, \quad (3a)$$

$$Q = \frac{(1-\phi-K_b/K_s)\phi K_s}{1-\phi-K_b/K_s + \phi K_s/K_f}, \quad (3b)$$

$$R = \frac{\phi^2 K_s}{1-\phi-K_b/K_s + \phi K_s/K_f}. \quad (3c)$$

The coefficient b appearing on the right hand side of Eqs. (1a), (1b), (2a), and (2b) corresponds to the viscous coupling factor, and the other inertial coefficients appearing on the left side of the above equations are given by the following formulas:

$$\hat{\rho}_{sf} = (1 - \alpha_\infty)\phi\rho_f, \quad (4a)$$

$$\hat{\rho}_f = \phi\rho_f - \hat{\rho}_{sf} = \alpha_\infty \phi\rho_f, \quad (4b)$$

$$\hat{\rho}_s = (1 - \phi)\rho_s - \hat{\rho}_{sf}, \quad (4c)$$

where ρ_s and ρ_f are the mass densities of the skeleton and of the interstitial fluid, and $\alpha_\infty \geq 1$ is the high frequency limit of the dynamic tortuosity of the considered porous media, which is a dimensionless parameter.[2]

As shown in Ref. 9, for $e^{-i\omega t}$ harmonic time dependency, the modified Biot equations can be easily derived by eliminating the fluid phase displacement vector U^f from the system of Eqs. (1a), (1b), (2a), and (2b) in terms of the skeleton displacement, which for simplicity is denoted as U (without the prefix s) in the rest of the paper, and the interstitial fluid pressure p:

$$\tilde{\rho}_s \omega^2 U + \nabla \cdot (\sigma^s - \alpha\phi p \delta) + \beta \ \nabla (\phi p) = 0, \quad (5a)$$

$$\nabla \cdot \left(\frac{1}{\tilde{\rho}_f \omega^2} \nabla (\phi p) - \beta \mathbf{U} \right) + \frac{\phi p}{R} + \alpha \nabla \cdot U = 0. \quad (5b)$$

The interstitial fluid displacement is related to the gradient of the acoustic pressure and the skeleton displacement by the following formula:

$$U^f = \frac{1}{\omega^2 \tilde{\rho}_f} \nabla (\phi p) - \frac{\tilde{\rho}_{sf}}{\tilde{\rho}_f} U. \quad (5c)$$

Equations (5a) and (5b) couple the skeleton displacement U to the interstitial fluid pressure p.

Effective masses $\tilde{\rho}_s$, $\tilde{\rho}_f$, and $\tilde{\rho}_{sf}$ appearing in Eqs. (5a)–(5c) are related to the structure and fluid mass densities ρ_s and ρ_f, to dimensionless parameters ϕ (porosity) and α_∞ (tortuosity), and to the viscous coupling factor b of the porous media,

$$\tilde{\rho}_{sf} = (1 - \tau)\phi\rho_f + \frac{b}{i\omega}, \quad (6a)$$

$$\tilde{\rho}_f = \tau\phi\rho_f - \frac{b}{i\omega}, \quad (6b)$$

$$\tilde{\rho}_s = (1-\phi)\rho_s - (1-\tau)\phi\rho_f - \frac{(1-\tau)^2\phi^2\rho_f^2}{\tilde{\rho}_f} - \frac{b}{i\omega}. \quad (6c)$$

According to Ref. 2, the viscous coupling factor b is given by the following formula:

$$b = \sqrt{1 - i\omega c^2 \frac{\alpha_\infty \rho_f}{2\phi\sigma}}, \quad (7a)$$

$$c = \frac{1}{\Lambda} \sqrt{\frac{8\alpha_\infty \eta}{\phi\sigma}}, \quad (7b)$$

where σ is the flow resistivity η to the viscosity of interstitial fluid and Λ is the viscous characteristic length.

Coefficients α and β couple the skeleton displacement U to the fluid pressure p in Eqs. (4a) and (4b). They correspond to the dimensionless stiffness and inertial coupling factors. They are given by

$$\alpha = 1 + \frac{Q}{R} = \frac{(1 - K_b/K_s)}{\phi}, \quad (8a)$$

$$\beta = 1 + \frac{\tilde{\rho}_{sf}}{\tilde{\rho}_f} = \frac{\rho_f}{\tilde{\rho}_f}. \quad (8b)$$

In general the bulk modulus K_b is very small compared to the bulk modulus K_s of the skeleton material ($K_b \ll K_s$), and for-

mula (8a) shows that the coefficient $\alpha\phi$ can be approximated by unity ($\phi\alpha \cong 1$).

The total stress tensor $\boldsymbol{\sigma}^{\text{tot}}$ applied to an elementary infinitesimal volume of the porous material is given by

$$\boldsymbol{\sigma}^{\text{tot}} = \boldsymbol{\sigma}^s - \phi\alpha p\,\boldsymbol{\delta}, \tag{9a}$$

where $\boldsymbol{\sigma}^s$ is the stress tensor inside the skeleton elastic material, which is given by

$$\widetilde{\boldsymbol{\sigma}} = (\lambda(\nabla \cdot U)\boldsymbol{\delta} + \mu(\nabla \cdot U + (\nabla \cdot U)^T)), \tag{9b}$$

where λ and μ are the Lame coefficients.

III. WAVE PROPAGATION IN POROUS MEDIA

The problem investigated in this paper involves the propagation of elastic and acoustic waves inside planar layers of porous material of finite thickness and infinite lateral dimensions. The explicit expressions of the pressure, the skeleton, and fluid displacements and stresses can be expressed in terms of three waves: two longitudinal waves and a shear wave. The global solution is obtained by superposition of the forward and backward traveling waves. For each porous layer there are six waves. Their complex amplitudes are determined by applying the appropriate boundary conditions.

The porous medium is supposed isotropic homogeneous and submitted to an incident unitary plane wave propagating in the $x\,y$ plane with an angle of incidence θ with respect to the x axis. In such configuration the incident plane wave has the following expression:

$$p_{\text{inc}}(x,y) = e^{ik_0(x\cos\theta + y\sin\theta)}, \tag{10}$$

where $k_0 = \omega/c_0$ is the acoustic wave number ω is the circular frequency, and c_0 is the speed of sound propagating in the surrounding acoustic medium at rest. In this case all field variables inside each porous layer are z independent and consequently have the following form:

$$p(x,y) = p(x)e^{ik_0\sin\theta.y},$$

$$U(x,y) = U(x)e^{ik_0\sin\theta.y}.$$

All equations can be written in the (x,y) plane, and since all variables have the same exponential dependency $e^{ik_0\sin\theta.y}$ in the lateral y direction, the problem reduces to a one-dimensional x dependency.

A. Wave equations

The skeleton displacement U has only two non-null components since the third component in the lateral z direction is identically null. The displacement U could be expressed in the following form:

$$\vec{U}(x,y) = \vec{\nabla}(\Phi(x)e^{ik_0\sin\theta.y}) + \vec{\nabla}\Lambda(\Psi(x)e^{ik_0\sin\theta.y}\vec{K}), \tag{11a}$$

where $\vec{K}$ is the unitary vector collinear to the z axis orthogonal to the xy plane of Fig. 1. Substitution of Eq. (11a) in the system of modified Biot's equations [Eqs. (3a)–(3c) and (4a)–(4c)] leads to the following system of three equations:

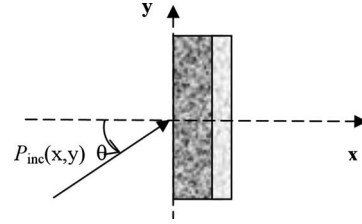$$\widetilde{\rho}_s\omega^2\Psi + \mu\,\Delta\Psi = 0, \tag{11b}$$

FIG. 1. Incident plane wave exciting porous layers.

$$\widetilde{\rho}_s\omega^2\Phi + (\lambda + 2\mu)\Delta\Phi + \gamma\phi p = 0, \tag{11c}$$

$$\frac{\phi\Delta p}{\widetilde{\rho}_f\omega^2} + \frac{\phi p}{R} - \gamma\Delta\Phi = 0, \tag{11d}$$

where

$$\gamma = (\beta - \alpha), \tag{12a}$$

$$\Delta = \frac{d^2}{dx^2} - k_0^2\sin^2\theta. \tag{12b}$$

Substitution of ϕp from Eq. (11b) to Eq. (11c) leads to the following equation:

$$\left\{\Delta^2 + \omega^2\frac{R}{\widetilde{\rho}_s}\left(\frac{\widetilde{\rho}_s}{(\lambda+2\mu)} + \frac{\widetilde{\rho}_f}{R} + \gamma^2\frac{\widetilde{\rho}_f}{(\lambda+2\mu)}\right)\Delta + \frac{\widetilde{\rho}_s\widetilde{\rho}_f}{(\lambda+2\mu)}\omega^4\right\}\Phi = 0. \tag{13}$$

Equation (13) can be written in the following form:

$$\{\Delta^2 + \omega^2 S\Delta + \omega^4 P\}\Phi = 0, \tag{14a}$$

where

$$S = \frac{R}{\widetilde{\rho}_s}\left(\frac{\widetilde{\rho}_s}{(\lambda+2\mu)} + \frac{\widetilde{\rho}_f}{R} + \gamma^2\frac{\widetilde{\rho}_f}{(\lambda+2\mu)}\right), \tag{14b}$$

$$P = \frac{\widetilde{\rho}_s\widetilde{\rho}_f}{(\lambda+2\mu)}. \tag{14c}$$

Equation (14a) can be factorized in the following form

$$\{(\Delta + k_1^2)(\Delta + k_2^2)\}\Phi = 0, \tag{15a}$$

where k_1 and k_2 are the wave numbers corresponding to longitudinal waves given by

$$k_1^2 = \frac{\omega^2}{c_1^2}, \tag{15b}$$

$$k_2^2 = \frac{\omega^2}{c_2^2}, \tag{15c}$$

where

$$c_1^2 = \frac{2}{(S + \sqrt{S^2 - 4P})}, \tag{15d}$$

$$c_2^2 = \frac{2}{(S - \sqrt{S^2 - 4P})}. \tag{15e}$$

c_1 and c_2 correspond to the speeds of slow and fast Biot's longitudinal waves.

The wave Eq. (11a) can be written as follows:

$$\frac{d^2 \Psi(x)}{dx^2} + (k_s^2 - k_0^2 \sin^2 \theta) \Psi(x) = 0, \tag{15f}$$

where

$$k_s^2 = \omega^2 \frac{\mu}{\tilde{\rho}_s} \tag{16a}$$

corresponds to the square of the shear wave number k_s. Equations (16a) and (16b) have two fundamental solutions,

$$\Psi^+(x) = e^{+i\gamma_s^+ x} \quad \text{and} \quad \Psi^-(x) = e^{-i\gamma_s^- x},$$

where γ_s^+ and γ_s^- are the two roots of the dispersion equation,

$$\gamma_s^2 + k_s^2 - k_0^2 \sin^2 \theta = 0. \tag{16b}$$

Equation (15a) shows that Eq. (13) has two solutions $\Phi_j(x)$ ($j=1,2$) satisfying

$$\left\{ \frac{d^2}{dx^2} + (k_j^2 - k_0^2 \sin^2 \theta) \right\} \Phi_j(x) = 0 \quad (j = 1,2). \tag{17a}$$

Equation (17a) also has two fundamental solutions,

$$\Phi_j^+(x) = e^{+i\gamma_j^+ x} \quad \text{and} \quad \Phi_j^-(x) = e^{-i\gamma_j^- x},$$

where γ_j^+ and γ_j^- are the two roots of the dispersion equation,

$$\gamma_j^2 + k_j^2 - k_0^2 \sin^2 \theta = 0. \tag{17b}$$

Once the shear wave numbers k_s and the longitudinal wave numbers k_1 and k_2 are computed, there are six independent fundamental solutions corresponding to the roots of Eqs. (16b) and (17b).

The displacement and the pressure fields relative to each fundamental solution can be computed using Eqs. (11a)–(11d). The global solution can be expressed in the following form:

$$\left\{ \begin{matrix} U \\ p \end{matrix} \right\} = \sum_{j=1}^{4} A_j \left\{ \begin{matrix} U \\ p \end{matrix} \right\}_{\Phi_j} + \sum_{l=1}^{2} B_l \left\{ \begin{matrix} U \\ 0 \end{matrix} \right\}_{\Psi_l}. \tag{18}$$

The six complex amplitudes can be determined using the boundary conditions at the layer's interfaces.

B. Boundary conditions

In this section boundary conditions are written for various interfaces.

Air/hard wall interface. The normal component of the acoustic (prefix 0) displacement is null,

$$U_z^0 = \frac{1}{\omega^2} \frac{dp^0}{dx} = 0.$$

Porous/hard wall interface. The porous medium can be considered to be sliding at the hard wall interface,

$$U_x^1 = U_x^{f1} = 0, \quad \tau_{xy}^1 = 0.$$

The porous medium can be fixed at the hard wall interface

$$U_x^1 = U_x^{f1} = 0; \quad U_y^1 = 0.$$

Air/porous interface. The boundary conditions depend on the nature of the interface, between the air and the porous medium. Since the interface could be impervious (closed cells) or perforated (open cells), the fluid domain is characterized by prefix (0) and the porous medium is characterized by prefix (1).

- perforated interface 0/1: 4 conditions:

$$(U_x^0 - U_x^1) = \phi^1 (U_x^{f1} - U_x^1),$$

$$p^0 = p^1,$$

$$-p^0 = \sigma_{xx}^1,$$

$$\tau_{xy}^1 = 0.$$

- impervious interface 0/1: 4 conditions:

$$U_x^0 = U_x^1,$$

$$(U_x^{f1} - U_x^1) = 0,$$

$$-p^0 = \sigma_z^1,$$

$$\tau_{xz}^1 = 0.$$

If the fluid is in direct contact with the porous medium (no facing film), the first equation corresponds to the continuity of the relative fluid flow through the interface. Hence the second equation expresses the continuity of the pressure since the interface is perforated. The third and fourth equations express the continuity of stresses.

If a weightless facing film separates the fluid and porous media domains, there are two cinematic conditions: the first equation expresses the continuity of the skeleton and external fluid normal components of displacements. The second equation determines that the air flow is null through the closed facing film, which is henceforth impervious. The third and fourth equations translate the continuity of stresses.

The facing mass could be taken into account by modifying the last two equations,

$$-p^0 = \sigma_x^1 - m\omega^2 U_x^1 \quad \text{and} \quad \tau_{xy}^1 - m\omega^2 U_y^1 = 0.$$

Porous/porous interface. The boundary conditions depend on the nature of the interface, between the two porous layers since the interface could be impervious (closed cells) or perforated (open cells). The left porous domain is characterized by prefix (1), and the right porous domain is characterized by prefix (2):

Coupling two porous layers requires six boundary conditions.

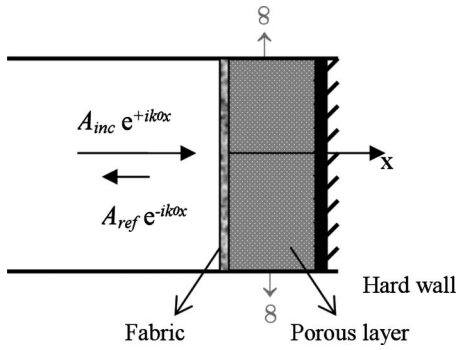- perforated interface 1/2:

$$U_x^1 = U_x^2,$$

FIG. 2. Impedance tube configuration.

$U_y^1 = U_y^2,$

$\sigma_x^1 = \sigma_x^2,$

$\tau_{xy}^1 = \tau_{xy}^2,$

$p^1 = p^2,$

$\phi^1(U_x^{f1} - U_x^1) = \phi^2(U_x^{f2} - U_x^2).$

- impervious interface 1/2:

$U_x^1 = U_x^2,$

$U_y^1 = U_y^2,$

$\sigma_x^1 = \sigma_x^2,$

$\tau_{xy}^1 = \tau_{xy}^2,$

$(U_x^{f1} - U_x^1) = 0,$

$(U_x^{f2} - U_x^2) = 0.$

The first four equations are identical for the direct and impervious weightless film interface. These equations are similar to the coupling between elastic layers. The first and second equations express the cinematic coupling of the skeleton displacements. The third and fourth equations express the continuity of stresses.

The two latter equations depend on the configuration considered. For direct coupling, we have pressure and air flow conservation across the interface. For coupling through an impervious interface, the air flow vanishes for both layers.

When the mass of the facing is taken into account, the last two equations must be modified as follows:

$$\sigma_x^1 = \sigma_x^2 - m\omega^2 U_x \quad \text{and} \quad \tau_{xz}^1 = \tau_{xz}^2 - m\omega^2 U_y.$$

IV. ABSORPTION COEFFICIENT

Two standing wave impedance tubes have been used to measure the AC of porous material samples (a small tube of 46 mm diameter and a large tube of square cross section of 600×600 mm^2).

As shown in Fig. 2, numerical simulations have been

TABLE I. Material properties.

Parameters	Foam	Fabric
Porosity ϕ	99.4%	13%[a]
Flow resistivity σ (N s m^{-4})	9045	66 639
Viscous length Λ (μm)	103	7.3[a]
Thermal length Λ' (μm)	197	12[a]
Tortuosity α_∞	1.02	1[a]
Skeleton density ρ_s (kg/m^3)	8.43	566.67
Young modulus E (kPa)	194.9	50[a]
Poisson ratio ν	0.42	0.3[a]
Damping factor η	5%	0[a]
Thickness (cm)	10	0.03
Fluid density ρ_0 (kg/m^3)	1.213	
Fluid celerity c_0 (m/s)	342.2	

[a]Parameters identified using analytical simulation and correlation with test data.

restricted to the normal incidence case, and results have been obtained using the material properties summarized in Table I. The acoustic AC α_{abs} is defined by the following expression:

$$\alpha_{abs} = 1 - \frac{A_{ref}^2}{A_{inc}^2}, \tag{19}$$

where A_{inc} and A_{ref} are, respectively, the amplitudes of the incident and reflected waves.

Measurements of the AC were made for bare foam and for foam covered by a fabric. Results were obtained in the frequency band ranging from 40 to 250 Hz for the large square tube and from 100 to 4000 Hz for the small circular tube. Two configurations were considered. The first one designated by (B) corresponds to the foam bonded to the termination of the tube. It was simulated by imposing the zero displacements of the skeleton and of the fluid. The second unbonded configuration designated by the symbol (U) is simulated by adding a thin (1 mm) air-gap between the foam and the tube termination.

Figure 3 shows good agreement between the experimental and the numerical results for a bare foam sample of 50 mm thick using both bonded and unbonded boundary conditions. However, to achieve such good agreement, it was necessary to tune the mechanical properties of the skeleton in
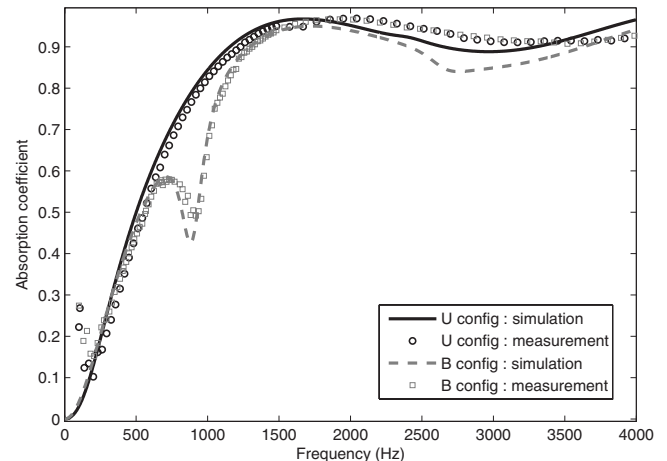

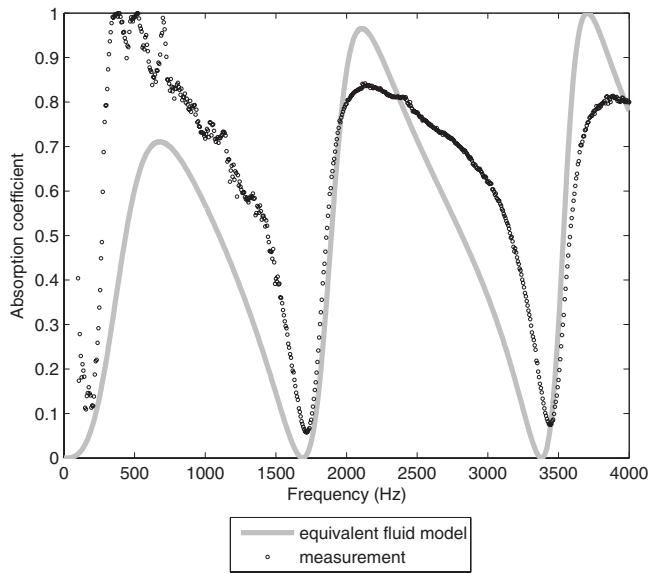FIG. 3. AC of a bare 5 cm foam layer (U and B configurations).

J. Acoust. Soc. Am., Vol. 125, No. 2, February 2009

Kanfoud et al.: Modeling of space lightweight acoustic protection   867

FIG. 4. AC measurement and simulation of a clamped fabric backed by a 10 cm cavity.

FIG. 5. Measurement of the effect of lateral mounting conditions on a 10 cm foam layer covered by a thin fabric.

order to adjust the resonance frequency of the porous sample since the skeleton resonance for the bonded case is controlled for one-dimensional propagation by the parameter $(\lambda+2\mu)$ appearing in Eq. (11c). This parameter can be modified by either changing Young's modulus or Poisson's ratio. Numerical results have been obtained using Young's modulus of Table I and a modified Poisson's ratio of 0.3 instead of 0.42. The resonance of the bonded foam occurs around 1 kHz, and there is no resonance for the unbonded configuration.

Three properties of the fabric were directly measured with acceptable precision: the flow resistivity, the mass density, and the thickness. The additional Biot parameters $(\phi, \alpha_\infty, \Lambda, \Lambda')$ and mechanical properties (E, ν) have been numerically identified using the best fit between the calculated and measured reflection coefficients for two configurations: (i) the fabric clamped in the small impedance tube and backed by an air gap of 100 mm depth and (ii) the foam covered by the fabric bonded to the termination of the small impedance tube.

Figure 4 shows the comparison between the measured and calculated ACs using the identified fabric parameters summarized in Table I. The frequencies corresponding to minimum and maximum values of the AC are well predicted, but the analytical model underestimates the first maximum level occurring at 500 Hz and overestimates the following maximum levels occurring at 2100 and 3750 Hz.

Here, the influence of lateral boundary conditions[11–13] has been studied experimentally from the 40 to 250 Hz range using the large square tube. Measurements were made on a 100 mm thick foam covered by fabric for different lateral boundary conditions. Figure 5 shows the influence of mounting conditions on the AC. When the fabric and the foam are simultaneously constrained in the impedance tube, the AC is higher in the low frequency band typically below 150 Hz and decreases above 150 Hz in comparison to the two other configurations, where the fabric is not constrained. Below 210
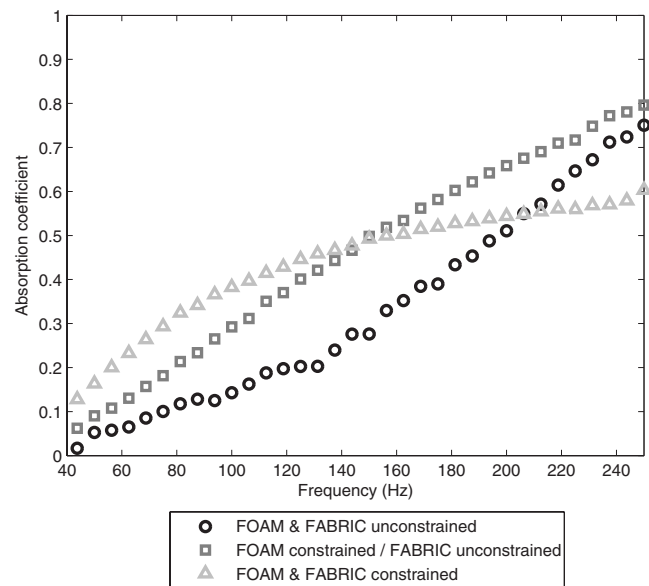
Hz, the third configuration corresponding to the unconstrained foam and fabric leads to the lowest level of the AC. Hence foam and fabric lateral constraints have similar effects. Experimental results show the strong influence of lateral boundary conditions on the AC for the low frequency range.

During the measurement of the AC of the fabric covered foam, very close attention has been paid to minimize the influence of lateral mounting conditions. Figure 6 shows very good agreement between measurements and calculations for the 100 mm thick bare foam and for the same foam sample covered by a fabric. However, to obtain such good agreement the structural loss damping of the foam has been increased to 18% in the numerical simulation. The fabric shifts the absolute maximum of the AC down from 750 to 500 Hz, leading to higher absorption below 500 Hz and lower absorption above 500 Hz. Figure 7(a) shows that the boundary condition between the foam and the tube termination has a significant influence only in the low frequency
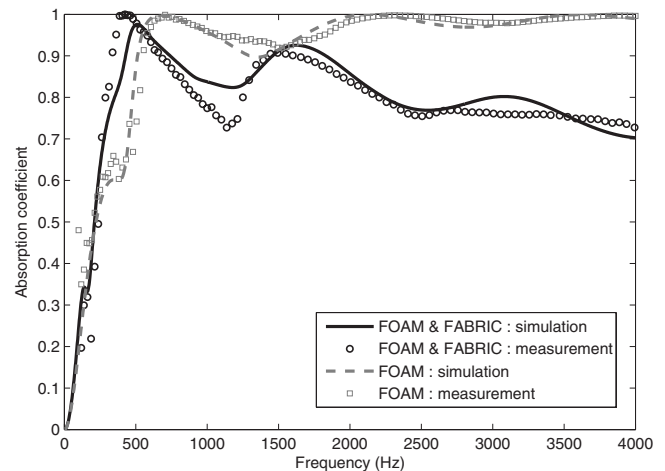

FIG. 6. AC of a bare 10 cm foam layer compared to the foam covered by a fabric.

Kanfoud *et al.*: Modeling of space lightweight acoustic protection
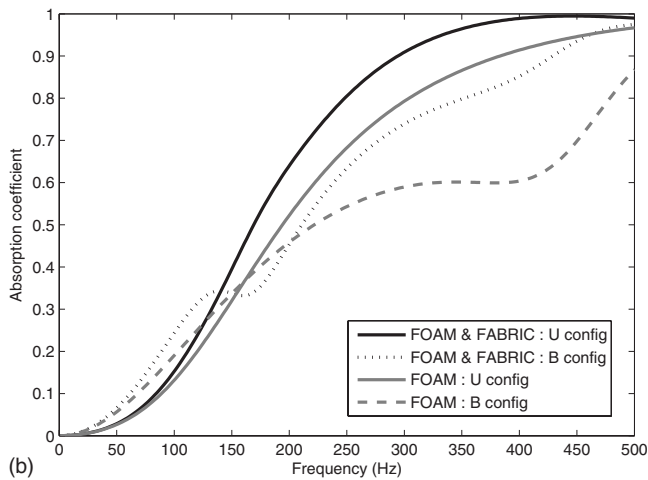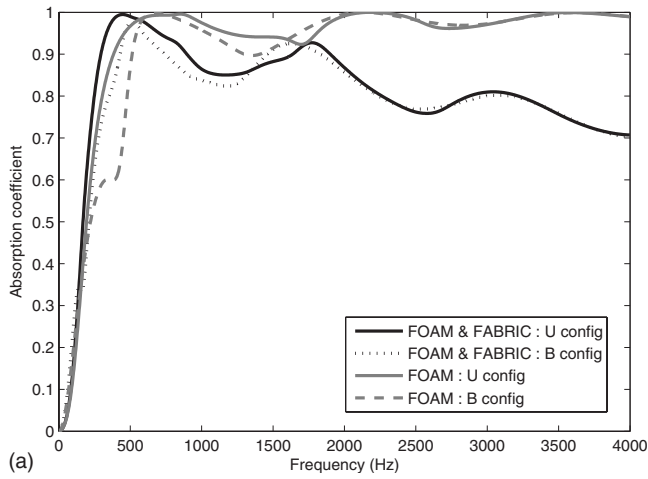
FIG. 7. (a) Simulation of the background mounting conditions on bare and covered 10 cm layers of foam (high frequencies). (b) Simulation of the background mounting conditions on bare and covered 10 cm layers of foam (low frequencies).

band below 750 Hz for the bare foam and 500 Hz for the foam covered by the fabric. The resonance of the skeleton is more pronounced for the bonded configuration. Figure 7(b) corresponds to a zoom below 500 Hz, showing that the unbonded configuration leads to higher absorption from 150 to 500 Hz. On the contrary, below 150 Hz, the bonded configuration leads to higher absorption. Globally, below 500 Hz the fabric increases significantly the level of AC compared to the bare foam.

A. The foam sensitivity to resistivity and Young modulus

In order to maximize the AC of the foam covered by the fabric in the low frequency band, a parametric study was conducted on foam material properties. It is well known that the parameters with most influence are the static air flow resistivity (σ) and the Young modulus (E) of the skeleton.

As shown in Fig. 8, the parametric study highlighted the existence of an optimal value of the resistivity, leading to an absolute maximum of the AC of the acoustic protection consisting of a fabric covered foam sample. The parametric
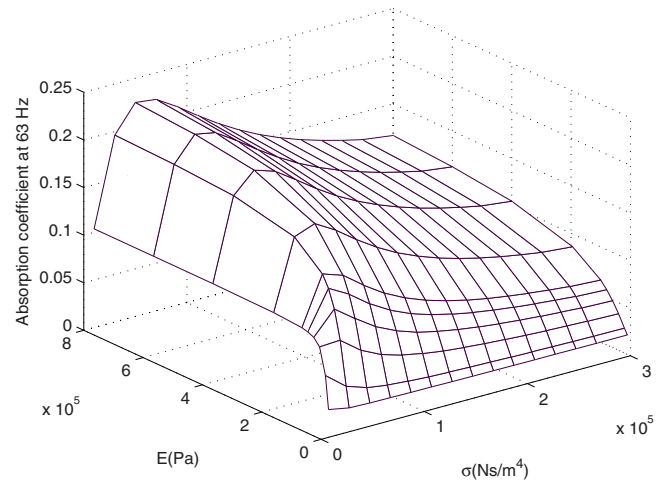

FIG. 8. Sensitivity of the absorption to the resistivity and the Young modulus at 63 Hz for the B configuration.

study was conducted at a particular frequency of 63 Hz for the bonded configuration. Figure 8 shows that a stiffer material leads to higher absorption.

Figure 9 shows variation with respect to the resistivity of the mean value of the AC averaged at the 63 Hz 1/3 octave band for two values of Young's modulus. The nominal value of Young's modulus of the foam and a higher value (ten times the nominal value) have been used. Both bonded and unbonded configurations have been studied, highlighting the influence of boundary conditions between the foam and the tube termination.

For the bonded configuration, the absolute maximum of the AC is obtained for optimal values of resistivity of 40 kN s m^{-4} for the nominal value of the Young's modulus and 50 kN s m^{-4} for the stiffer foam (ten times). The unbonded configuration requires very high resistive foams. In this case the optimal value of resistivity is located above
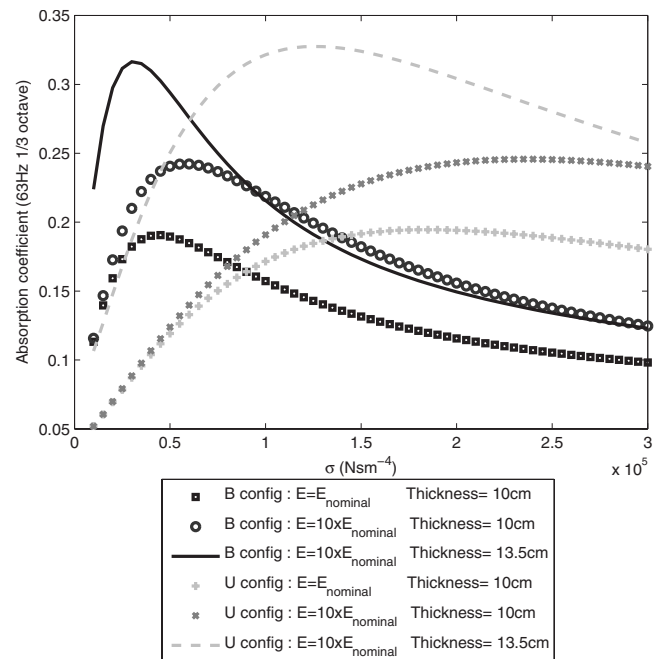

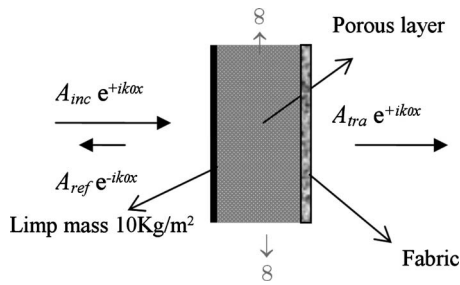FIG. 9. Sensitivity of the AC to the resistivity at the 1/3 octave of 63 Hz.

J. Acoust. Soc. Am., Vol. 125, No. 2, February 2009

Kanfoud *et al.*: Modeling of space lightweight acoustic protection   869

FIG. 10. Transmission loss (TL) configuration.

150 kN s m^{-4}. As expected, Fig. 9 shows that increasing the foam thickness from 10 to 13.5 cm leads to further improvement of the AC.

V. TRANSMISSION LOSS AND NOISE REDUCTION FACTORS

Many sound transmission studies have been conducted on structures lined with porous materials. Bolton et al.,[3] Bolton and Shiau,[4,5] Bolton and Green,[14] and Becot and Sgard[15] investigated an analytical model to predict sound transmission through double structure panels lined with porous layers simulating a simplified aircraft fuselage. Other researchers developed various numerical methods to analyze sound radiation and transmission by elastic structures covered by porous elastic layers.[16,17]

Here, the proposed analytical model is applied to calculate the TL and the NR factors of infinite structure panels lined by a foam layer covered by a fabric. The structure panels are represented by a limp mass.

The simple configurations considered try to derive rules for the design of lightweight acoustic protection to be integrated in the fairing of space launchers. In this context, the noise TL coefficient is calculated (Fig. 10) by considering a laterally infinite impervious limp mass of 10 kg/m^2, covered by a porous layer as shown below. The porous layer is 10 cm thick. Nominal parameters given in Table I are used. A Poisson's ratio of $\nu=0.3$ has been used since it led to a better correlation with measurements.

The TL is defined by the following formula:

$$\text{TL} = 10 \log \frac{A_{\text{inc}}^2}{A_{\text{tra}}^2}, \tag{20}$$

where A_{inc} and A_{tra} are the amplitudes of incident and transmitted acoustic waves.

The NR factor simulates the noise level inside a laterally infinite cavity of finite width (Fig. 11) limited by two panels
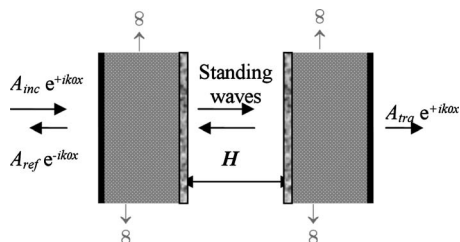

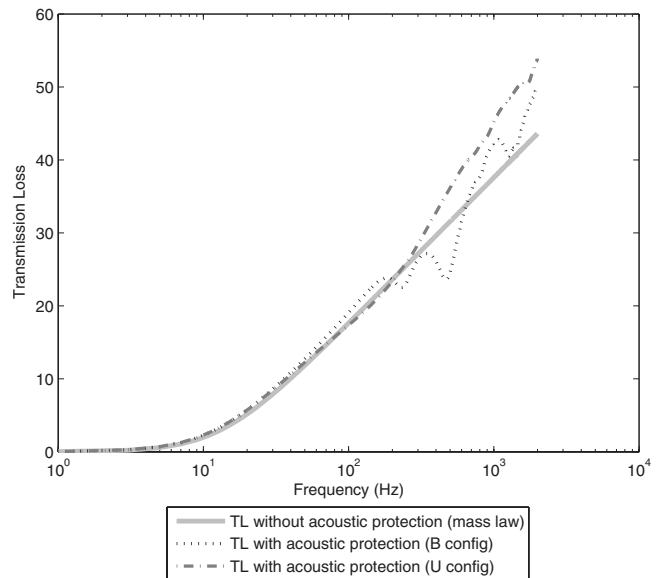FIG. 11. Noise reduction (NR) configuration.

FIG. 12. TL of a limp mass lined with an absorbing complex.

represented by limp masses covered by the optimized acoustic protection. The NR is defined by the following formula:

$$\text{NR} = 10 \log \frac{A_{\text{inc}}^2}{P_{\text{int}}^2}, \tag{21}$$

where P_{int}^2 is given by

$$P_{\text{int}}^2 = \frac{1}{H} \int_0^H p_{\text{int}}(x) p_{\text{int}}^*(x) dx, \tag{22}$$

where $P^*(x)$ is the complex conjugate of the internal pressure $P(x)$.

Figure 12 shows that below 100 Hz, the foam has very little effect on the TL since the curve coincides with the mass law. Above 100 Hz, the porous complex enhances the TL in the case of the unbonded configuration. For the bonded configuration, local frequency drops of the TL curve are observed at porous layer resonance frequencies. A parametric study has been carried out for fixed mechanical properties of the skeleton. It shows that the Biot's parameters related to the propagation of the airborne wave in the porous medium have very little effect on the TL curve. The structural resonance frequencies vary mainly with mechanical properties of the skeleton of the porous layer.

Figure 11 shows an air-filled cavity of width H, limited at each side by a limp mass layer covered by a porous layer simulating the acoustic protection. Figure 13 superimposes TL curves ($H \to \infty$) to the NR curves obtained for a cavity of finite width ($H=1$ m).

The NR curves obtained with and without the porous layer oscillate around the corresponding TL curves. Without the porous layer, sharp peaks appear at the resonances of the acoustic cavity. The amplitudes of these picks are strongly attenuated when limp mass layers are covered by the porous layers simulating the acoustic protection. When the limp mass is covered by the porous material layers, the NR is very close to the TL curve above 500 Hz. Below 500 Hz the
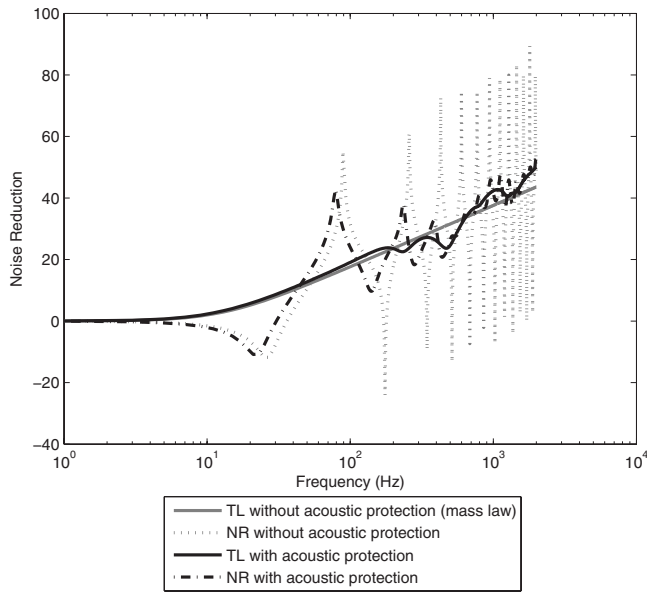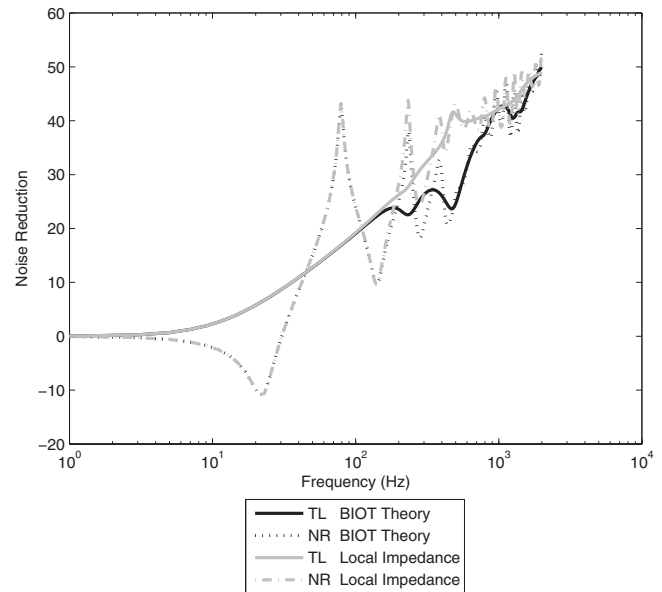
FIG. 13. NR of a cavity of width $H = 1$ m.

FIG. 14. Comparison of local impedance and Biot models.

optimized porous layer is still very efficient. It attenuates the first acoustic mode by 10 dB, the second by 30 dB, and the third by more than 40 dB.

In the current state of the art, NR factors of space structures[18] are predicted using the LAI measured in an impedance tube. The value of the local impedance is determined by placing the porous layer at the termination of an impedance tube. The associated boundary conditions at the interface of the acoustic cavity are written as follows:

$$\frac{1}{\rho_0} \frac{dp_{\text{int}}}{dx} - \frac{i\omega}{Z} p_{\text{int}} = -\omega^2 U^s, \qquad (23a)$$

$$p_{\text{ext}} - p_{\text{int}} = -\omega^2 m U^s, \qquad (23b)$$

where ρ_0 is the mass density of air, Z is the LAI of the porous layer bonded at the termination of the impedance tube, p_{int} is the internal acoustic pressure, p_{ext} is the external pressure (sum of incident and reflected waves), and U^s is the displacement of the limp mass m per unit area.

Results corresponding to the LAI model by applying boundary conditions (23a) and (23b) are compared to those obtained using the present modified Biot model. Figure 14 superimposes TL and NR curves corresponding to LAI and present Biot models.

Below 200 Hz, the curves corresponding to the two models coincide. The two models diverge between 200 and 2000 Hz because the LAI model does not predict the resonances of the porous layer and consequently overestimates the NR and the TL. Above 2000 Hz the two models start to converge again.

VI. CONCLUSION

A modified system of Biot equations has been solved analytically for infinite planar layers of porous media. Various acoustic indicators such as the acoustic absorption coefficient (AC), TL, and NR factors have been computed for different configurations. The sensitivity of the acoustic AC to

the boundary conditions, to the variation of Biot's acoustical parameters, and to the mechanical properties of the skeleton has been thoroughly studied. The analytical results have been validated by impedance tube measurements, showing good agreement between experimental and numerical results.

This study demonstrated that the mounting boundary conditions (lateral and longitudinal) influence the AC in the low frequency band. The analytical model developed permitted a rapid parametric study to be made of the influence of the two most significant parameters, which are the static air flow resistivity and the Young modulus of the porous material. For a given low frequency band (1/3 octave), an optimal value of the flow resistivity leads to a maximum value of the AC. Stiff materials (high Young's modulus) lead to higher absorption at the low frequency range. For high frequency bands, the increase in resistivity leads to an enhancement in the AC. In low frequency bands, the absolute value of the maximum of the AC is very sensitive to the mechanical properties of the skeleton and the boundary conditions.

The developed method allowed the calculation of the TL factor of limp mass panels covered by the optimized acoustic protection composed by two layers (foam and fabric) of porous materials. It is demonstrated that the TL obtained with the acoustic protection is always higher than the TL curve of the classical mass law, except at the first resonances of the foam layer, where the TL curve drops locally.

The proposed method also permits the calculation of the NR factor of a simplified structure composed of two limp mass layers covered by the optimized acoustic protection and containing an acoustic cavity of finite width. It has been demonstrated that the optimized acoustic protection is very efficient. It allows strong damping of internal acoustic resonances.

In addition the developed method allowed the analysis of results obtained using the approximate LAI model, which gives good results in low and high frequency limits. In the medium frequency range, the LAI model is less accurate than

the present modified BIOT model since it overestimates the NR factor near the resonances of the foam layer.

ACKNOWLEDGMENTS

[1] M. A. Biot, "Theory of propagation of elastic waves in a fluid-saturated porous solid I: Low-frequency range II: Higher frequency range," J. Acoust. Soc. Am. **28**, 168–191 (1956).

[2] J. F. Allard, *Propagation of Sound in Porous Media: Modelling Sound Absorbing Materials* (Elsevier, New York, 1993).

[3] J. S. Bolton, N. M. Shiau, and Y. J. Kang, "Sound transmission through multi-panel structures lined with elastic porous materials," J. Sound Vib. **191**, 317–347 (1996).

[4] J. S. Bolton and N. M. Shiau, "Oblique incidence sound transmission through multi-panel structures lined with elastic porous material," in Proceedings of the 11th AIAA Aeroacoustics Conference, Sunnyvale, CA (October 1987), Paper No. AIAA-87-2660, pp. 19–21.

[5] J. S. Bolton and N. M. Shiau, "Random incidence sound transmission through multi-panel structures lined with elastic porous material," in Proceedings of the 12th AIAA Aeroacoustics Conference, San Antonio, TX (October 1989), Paper No. AIAA-89-1048, pp. 10–12.

[6] G. Bonnet, "Basic singular solutions for a poroelastic medium in the dynamic range," J. Acoust. Soc. Am. **82**, 1758–1762 (1987).

[7] N. Atalla, R. Panneton, and P. Debergue, "A mixed displacement-pressure formulation for poroelastic materials," J. Acoust. Soc. Am. **104**, 1444–1452 (1998).

[8] P. Debergue, R. Panneton, and N. Atalla, "Boundary conditions for the weak formulation of the mixed (u,p) poroelasticity problem," J. Acoust. Soc. Am. **106**, 2383–2390 (1999).

[9] M. A. Hamdi, L. Mebarek, A. Omrani, and N. Atalla, "An efficient formulation for the analysis of acoustic and elastic waves propagation in porous-elastic materials," in ISMA 25, International Conference on Noise and Vibration Engineering, Katholieke Universiteit Leuven, Belgium (13–15 September 2000).

[10] N. Atalla, M. Hamdi, and R. Panneton, "Enhanced weak integral formulation for the mixed (U,p) porous-elastic equations," J. Acoust. Soc. Am. **109**, 3065–3068 (2001).

[11] D. Pilon and R. Panneton, "Behavioral criterion quantifying the effect of circumferential air gaps on porous materials in the standing wave tube," J. Acoust. Soc. Am. **116**, 344–356 (2004).

[12] B. H. Song, J. S. Bolton, and Y. J. Kang, "Effect of circumferential edge constraint on the acoustical properties of glass fiber materials," J. Acoust. Soc. Am. **110**, 2902–2916 (2001).

[13] A. Cummings, "Impedance tube measurements on porous media: The effect of air-gaps around the sample," J. Sound Vib. **151**, 63–75 (1991).

[14] J. S. Bolton and E. R. Green, "Normal incidence sound transmission through double-panel systems lined with relatively stiff, partially reticulated polyurethane," Appl. Acoust. **39**, 23–51 (1993).

[15] F. X. Becot and F. Sgard, "On the use of poroelastic materials for the control of the sound radiated by a cavity backed plate," J. Acoust. Soc. Am. **120**, 2055–2066 (2006).

[16] N. Atalla, F. Sgard, and C. K. Amedin, "On the modelling of sound radiation from poroelastic materials," J. Acoust. Soc. Am. **120**, 1990–1995 (2006).

[17] R. Panneton and N. Atalla, "Numerical prediction of sound transmission through finite multilayer systems with poroelastic materials," J. Acoust. Soc. Am. **100**, 346–354 (1996).

[18] H. Defosse and M. A. Hamdi, "Vibro-Acoustic study of Ariane V launcher during lift off," in Proceeding of the 29th International Congress on Noise Control Engineering, Inter-Noise 2000, Nice, France (27–30 August 2000).